International Journal of Heat and Mass Transfer 52 (2009) 2740–2748

Contents lists available at ScienceDirect

International Journal of Heat and Mass Transfer

journal homepage: www.elsevier.com/locate/ijhmt

# Heat transfer from a turbulent swirling inverse diffusion flame to a flat surface

H.S. Zhen, C.W. Leung *, C.S. Cheung

*Department of Mechanical Engineering, The Hong Kong Polytechnic University, Hung Hom, Hong Kong, China*

ARTICLE INFO

*Article history:*
Received 12 August 2008
Received in revised form 23 December 2008
Available online 4 March 2009

*Keywords:*
Inverse diffusion flame
Induced-swirl
Flame impingement
Heat transfer

ABSTRACT

The heat transfer characteristics of a turbulent and swirling inverse diffusion flame (IDF) impinging vertically normal to a flat surface were investigated experimentally. The heat flux was measured by a heat flux sensor, Vatell HFM-6D/H. The effects of Reynolds number, overall equivalence ratio, nozzle-to-surface distance $H$ and swirl number on the heat flux distributions were examined. The comparison of heat transfer of impinging IDFs with and without swirl was also conducted.

The experimental results showed that the swirling effect influences the local heat flux in three ways. (1) The heat transfer at the stagnation point is severely suppressed. (2) The peak of local heat flux dwells at a radial distance from the stagnation point. (3) The radial position of peak local heat flux shifts farther away from the stagnation point with increasing $H$. There exists an optimum value of $H$ at which the heat transfer to the target surface is the maximum and the optimum $H$ increases with increasing $\Phi$ while the Reynolds number and the swirl number are unchanged.

The comparison of IDFs revealed that the swirling IDF has more complete combustion and thus it is accompanied by higher heat transfer rates at small $H$ at which there exists a cool core in the case of the non-swirling IDF. The IDF, however, has worse heat transfer at higher $H$ where the non-swirling IDF achieves complete combustion while the swirling IDF has been cooled by the entrained ambient air.

Upon comparing the swirling and non-swirling IDFs at the same $Re$ and $\Phi$, their respective optimum $H$ showed an unfavorable effect of swirl on the overall heat transfer rate which has a reduction of up to 25% in the swirling IDF compared with the non-swirling IDF.



## 1. Introduction

The thermal performance of a flame impingement system is affected by factors such as burner style, flame jet properties, impingement surface condition and configuration between the burner nozzle and the surface. Due to the complexity of the problem, there is a continued effort in investigating the heat transfer characteristics of impinging flames.

Extensive literature reviews on impinging flame jets have been performed by Jambunathan et al. [1], Baukal and Gebhart [2,3] and Chander and Ray [4]. Numerous studies have been carried out to understand the characteristics of the flame impingement system, ranging from the flow and flame structure [5–7], and the heat transfer characteristics [8–12], to the pollutants emission characteristics [13,14]. In most of these studies [5,9–11,13,14], premixed or partially pre-mixed flame was used as the impinging flame due to the high flame temperature and the low soot emission. In recent years, inverse diffusion flames have received increasing attention due to its ability to operate in a wide range of fuel and air flow rates without occurrence of flashback or lift-off. The feasibility of using an IDF for impingement heating has been studied in Refs. [6–8,12], which reported that the IDF has a bell-shaped radial heat flux distribution at high nozzle-to-surface distance, similar to that of conventional circular impinging pre-mixed flame jets, and that the heat flux in the stagnation region drops heavily at low nozzle-to-surface distance because of the presence of a cool core at low flame heights.

There have been some published papers on the heat transfer characteristics of single and multiple impinging swirling isothermal jets. Ward and Mahmood [15] used naphthalene sublimation technique to investigate the effect of heat and mass transfer on a flat surface from a swirling impinging jet. They found that the measured radial distribution of local Nusselt number was slightly more uniform than that for a conventional impinging jet, but its values were significantly lower, particularly in the vicinity of the stagnation point. They concluded that the swirl has an unfavorable effect on heat transfer in terms of both local and average value of the parameters tested. The same authors [16] examined the effect of swirl in a rectangular nozzle array. In this case, the interaction between neighboring co-rotating jets led to an overall heat transfer enhancement. Such an enhancement was observed only at the swirl number range of 0.12–0.24 when the nozzle array is relatively close to the impingement surface. Huang and El-Genk [17]

* Corresponding author. Fax: +852 23654703.
*E-mail address:* mmcwl@polyu.edu.hk (C.W. Leung).

0017-9310/$ - see front matter © 2009 Elsevier Ltd. All rights reserved.
doi:10.1016/j.ijheatmasstransfer.2008.12.010

**Nomenclature**

| | |
|---|---|
| $a$ | distance from the exit, m |
| $A_e$ | exit area, $m^2$ |
| $A_t$ | tangential inlet area, $m^2$ |
| $d$ | exit diameter, m |
| $D_0$ | chamber diameter, m |
| $D_t$ | tangential inlet diameter, m |
| $G'_x$ | axial flux of linear momentum, kg m $s^{-1}$ |
| $G\varphi$ | axial flux of angular momentum, kg $m^2$ $s^{-1}$ |
| $H$ | nozzle-to-surface distance, m |
| $H/d$ | non-dimensional nozzle-to-surface distance |
| $h_{max}$ | peak of each heat flux profile, $kW/m^2$ |
| $L$ | chamber length, m |
| $L_{div}$ | length of the divergent outlet, m |
| $\dot{q}_{local}$ | local heat flux, $kW/m^2$ |
| $\dot{q}$ | area-integrated heat flux, kW |
| $\dot{Q}_a$ | axial volumetric flow rate, $m^3$ $s^{-1}$ |
| $\dot{Q}_t$ | tangential volumetric flow rate, $m^3$ $s^{-1}$ |
| $\dot{Q}_{fuel}$ | volumetric flow rate of LPG, $m^3$ $s^{-1}$ |
| $R_0$ | chamber radius, m |
| $R$ | radial distance from the stagnation point, m |
| $R/d$ | non-dimensional radial distance from the stagnation point |
| $Re$ | Reynolds number |
| $S$ | actual swirl number |
| $S'$ | geometric swirl number |
| $\Phi$ | overall equivalence ratio |
| $\eta$ | heat transfer efficiency, % |
| $\rho_{fuel}$ | density of LPG, kg $m^{-3}$ |
| $LHV_{fuel}$ | lower heating value of LPG, J $kg^{-1}$ |

used a swirl generator made of a cylindrical plug with four narrow channels to provide swirl to single and multiple impinging air jets. Their results demonstrated improvement in the radial uniformity and large increases in the local and average Nusselt number. Owsenek et al. [18] carried out numerical investigations of impinging jet with superimposed swirl. However, their study was limited to the laminar flow regime. Lee et al. [19] tested on a vane-type swirl generator and measured the local Nusselt number for a swirling round turbulent jet impinging on a flat plate. They found that the effect of swirling jet flow is mainly significant near the stagnation region and for small nozzle-to-surface distance. The average Nusselt number is larger than that with non-swirling flow. However, for large nozzle-to-surface distance, the effect of swirling jet flow is rarely seen and the average Nusselt number can be lower than that with non-swirling flow. They also indicated a uniform distribution of the local Nusselt number at large nozzle-to-surface distances and large swirl numbers. The experimental results from Yuan et al. [20] revealed that the swirling jet causes a significant change of the heat transfer distribution. The heat transfer in the stagnation region deteriorates to some extent and rises in the wall jet region, thus the radial uniformity is improved.

Only a few studies of the heat transfer characteristics of single and multiple impinging swirling flame jets have been made. Huang et al. [21] showed that a circular laminar pre-mixed flame jet with induced-swirl has a more uniform heat flux distribution and higher temperatures when compared with the flame jet without swirl. An array of three identical laminar pre-mixed flames with induced-swirl was developed by Zhao et al. [22], who suggested that under low-pressure and low-Reynolds-number conditions, a swirling flame jet array can achieve more complete combustion at shorter nozzle-to-surface distance and provides more uniform heat transfer on the target surface. Furthermore, the heating efficiency is enhanced when induced-swirl is applied.

Earlier studies have enriched our knowledge of the heat transfer characteristics of impinging swirling isothermal and flame jets. However, previous studies are mostly performed on laminar jets or pre-mixed flame jets with low swirl intensities which do not involve flow recirculation. The application of high-swirl in a flame jet has many advantages such as rapid mixing of fuel and oxidizer, enhancement of flame stability, broader operational limits and reduced soot formation [23]. Thus, the main purpose of this study is to investigate the heat transfer characteristics of a turbulent inverse diffusion flame impinging vertically normal to a flat surface with induced high-swirl. The swirling effect on the heat transfer is to be identified in such a way that focus will be put on the influences of different operational parameters including Reynolds number, overall equivalence ratio, nozzle-to-surface distance and swirl number on the heat flux distribution.

## 2. Experimental set-up and method

Fig. 1 shows the IDF burner used in this study. It was designed based on recommendations in Ref. [23] to reduce pressure loss and ensure the formation of an internal recirculation zone (IRZ) in the swirling IDF. The burner is made of brass and contains a swirl chamber in which air enters tangentially to induce a rotational motion. There are two tangential air inlets to ensure an even flow structure inside the chamber and one axial air inlet at the bottom of the swirl chamber so that the degree of swirl can be altered easily by adjusting the ratio between tangential and axial flows. The swirling air flows through a contracted throat section and then emerges from a divergent outlet. The divergent outlet aims to enlarge the recirculation zone and improve the flame stability. There is a 12-mm-diameter central air port, which is the contracted section of the swirl chamber, and twelve 2.4-mm-diameter fuel ports arranged evenly around the air port. The axis of each fuel port is aligned at an angle of 45° to the axis of the air port to ensure that the fuel jets will collide and mix with the air jet. LPG consisting of 70% butane and 30% propane is used as the fuel (representing the standard composition of LPG available in Hong Kong). Both the LPG and the compressed air are metered and monitored by calibrated flowmeters before entering the burner.

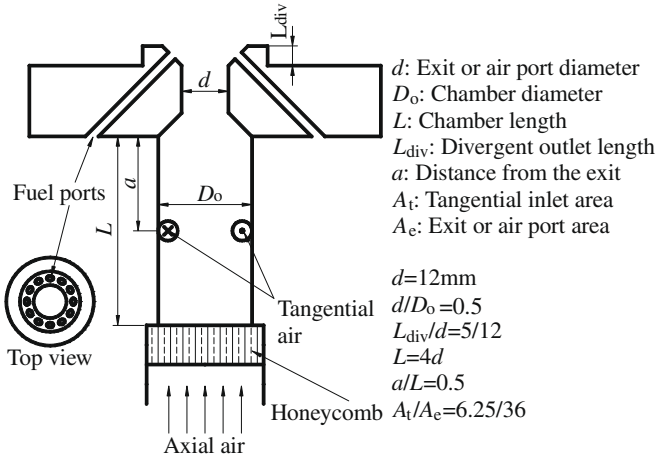


**Fig. 1.** Sketch of IDF burner.

Claypole and Syred [24] suggested a non-dimensional geometric swirl number $S'$ which can be satisfactorily and conveniently calculated from the geometry of a swirl generator involving tangential and axial flows:

$$S' = \frac{G_\varphi}{G'_x R_0} = \frac{(D_0 - D_t)D_0}{2D_t^2}\left(\frac{\dot{Q}_t}{\dot{Q}_t + \dot{Q}_a}\right)^2 \quad (1)$$

According to Ref. [23], internal recirculation zones are generally formed when the actual swirl number $S$ exceeds 0.6. For the swirling flame in this study, the internal recirculation zone is formed when the geometric swirl number $S'$ exceeds 2.4. The term 'swirl number' refers to $S'$ in this paper unless otherwise stated.

The experimental apparatus is schematically illustrated in Fig. 2. The burner is placed on a 3D positioner which can locate the burner at any position in space. A screen mesh is used to enclose the flame for minimization of the disturbance from the surrounding air flow. The target surface is a water-cooled copper plate with a surface area of $600 \times 600\ mm^2$ and 12 mm thick. It is evenly cooled on the backside by a cooling water jacket. The temperature of cooling water is maintained at 38 °C by a thermostat to avoid condensation. The top plate covering the cooling water jacket is made of plexi-glass to render the water flow visible. At the center of the copper plate, a heat flux sensor is attached to measure the local heat flux from the flame to the plate. It is a small ceramic heat flux transducer (Vatell Corporation, Model HFM-6D/H) with an effective sensing area of $2 \times 2\ mm^2$. It is mounted in the copper plate according to the manufacturer's specifications with a ±0.01 mm dimensional tolerance to ensure that the sensor and the plate are in the same alignment and that the sensor surface is flush with the front side of the plate facing the flame. The standard coating for the face of the sensor is zynolyte, which is a high temperature black coating with a 0.94 emissivity. The voltage signal is recorded by a stand-along IOtech data acquisitor after having been amplified by an AMP-6 amplifier with an accuracy of ±1.5%. The sensor is supplied with a NIST traceable calibration certificate that provides all the information necessary to convert signals from the sensor to heat flux values with an accuracy of ±3%.

During the experiments, the swirling IDF impinged vertically normal to the copper plate. The carefully arranged experiments enabled individual investigation of the effects of different operational parameters including $Re$, $\Phi$, $H$ and $S'$ on the heat transfer characteristics of the IDF impingement system, in terms of the radial heat flux distribution on the target surface. Tests were firstly carried out to identify the optimum nozzle-to-surface distance $H_{optimum}$ at $Re = 8000$, $\Phi = 1.4$ and $S' = 9.12$. Secondly, variation of the overall equivalence ratio from 1.0 to 2.0 was performed at $Re = 8000$, $H = H_{optimum}$ and $S' = 9.12$. Thirdly, the Reynolds number was varied from 6000 to 10000 at $\Phi = 1.5$, $H = H_{optimum}$ and $S' = 9.12$. Fourthly, variation of the swirl number from 4.56 to 9.12 was implemented at $Re = 8000$, $\Phi = 1.5$ and $H = H_{optimum}$. Finally, a non-swirling IDF produced by the same burner was studied for the purpose of comparison. In this paper, $Re$ refers to the air jet Reynolds number. It is evaluated based on the air jet diameter and the air jet velocity. The overall equivalence ratio $\Phi$ which is evaluated based on the mass flow rate of the central air jet and the mass flow rate of the fuel jets to indicate the relative strength of the air and fuel supply in relation to the stoichiometric air fuel ratio. Both the nozzle-to-surface distance $H$, defined as the vertical distance from the burner rim to the copper plate, and the radial distance from the stagnation point $R$, are normalized by the diameter of the central air port $d$.

All the radial heat fluxes were measured along a radial distance of 180 mm, starting from the stagnation point, at 4 mm interval for the first 40 mm distance, 6 mm for the next 60 mm and 8 mm for the last 80 mm. Each heat flux value was registered only after a steady state has been achieved. Based on the radial heat flux distribution, the area-integrated heat flux or the overall heat transfer rate and the heat transfer efficiency can be calculated from Eqs. (2) and (3), respectively:

$$\dot{q} = \int\int^{A} \dot{q}_{local}\,dA = 2\pi \int_0^R \dot{q}_{local} r\,dr \quad (2)$$

$$\eta(\%) = \frac{\text{Output}}{\text{Input}} \times 100\% = \frac{\dot{q}}{\dot{Q}_{fuel}\rho_{fuel}LHV_{fuel}} \times 100\% \quad (3)$$

The area-integrated heat flux was obtained by integrating the radial distribution of the local heat flux within a circular zone of 180 mm radius centered at the stagnation point. The radial distance of 180 mm was chosen because in most cases, the local heat flux would have decayed by more than 90% beyond $R = 180$ mm. An uncertainty analysis was carried out with the method proposed by Kline and McClintock [25]. Using a 95% confidence level, the maximum and minimum uncertainties in heat flux were found to be 15% and 0.2%, respectively.

## 3. Results and discussions

### 3.1. Flame structure

The flame image of the swirling IDF in the open environment at $Re = 8000$, $\Phi = 1.4$ and $S' = 9.12$ is shown in Fig. 3. The open swirling IDF is a peach-shaped flame and can be separated into three zones. Zone 1 is the internal recirculation zone (IRZ), which is formed by the axial adverse pressure gradient induced by the swirl [23]. Zones 2 and 3 are the flame boundaries in the lower and upper sections, respectively. For all the experimental conditions studied in the present work, Zones 1 and 3 have a color of sky-blue and the color of Zone 2 is navy-blue, showing that the whole flame behaves as a pre-mixed flame. A flow visualization technique was used to investigate the flame structure. It was achieved by inserting a thin

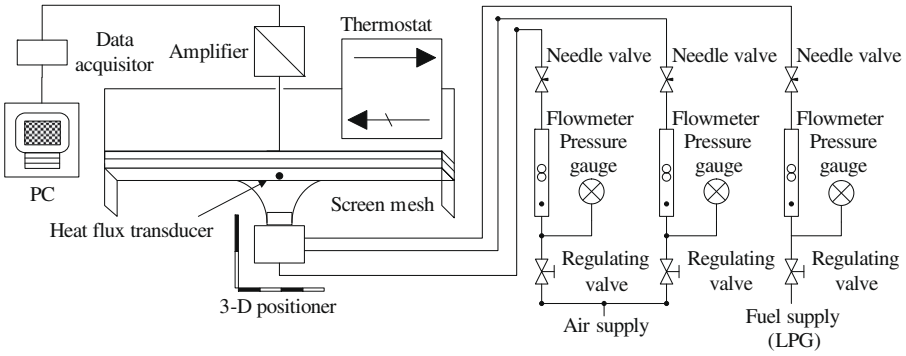


**Fig. 2.** Experimental set-up for heat flux measurement.

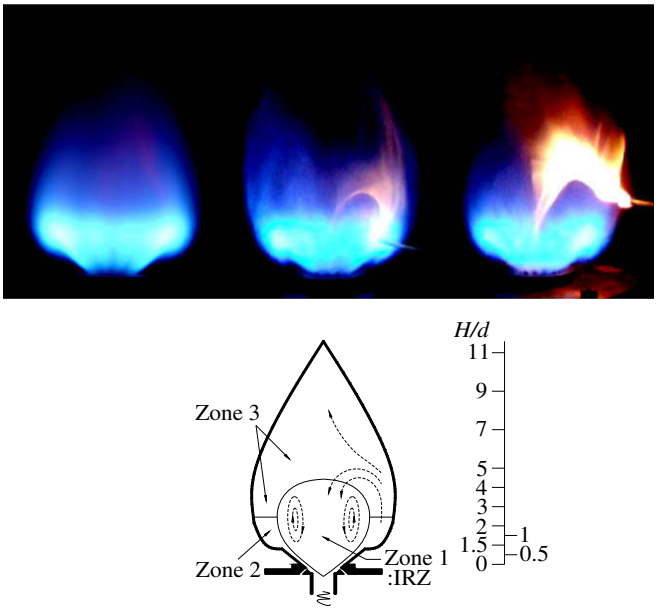


**Fig. 3.** Structure of open swirling IDF and images of flow visualization at $Re$ = 8000, $\Phi$ = 1.4 and $S'$ = 9.12.

wooden rod into the flame to dye the fluid color to yellow. The small yellow blaze introduced by combusting the rod followed the mainstream and acted as streaklines. Thus, the local flow fields were visible to the naked eyes. By placing the rod in different positions in the flame and combining the separate local flow fields, the complete flow field or the flame structure could be obtained. The identified flame structure and some images of the local flow field visualization are also shown in Fig. 3. From such images, it is observed that the fluid particles come out of the burner nozzle mainly through Zone 2, and then a large portion of the fluid particles in Zone 3 are diverged towards the burner axis and recirculate towards the burner exit to form a reverse flow in Zone 1. This is consistent with the results of Ref. [26], which studied the mean flow structures in strongly swirling flows. The literature stated that the reverse flow boundary is shaped like an ellipse, with the mean gas flow above the boundary going upstream and the mean gas flow below these lines going downstream.

When this swirling IDF impinged onto the target surface, the development of the flame along the vertical direction was impeded and the target surface forced the flame to spread outwards radially. Thus the impinging swirling IDF spreads outwards radially at a faster rate compared to that of the open swirling IDF. This higher spreading rate results in a higher level of entrainment of ambient air, which in turn results in an additional expansion of the vertical flame before its impingement on the target surface. The additional expansion refers to the enlarged cross-sectional area of a particular portion of the flame, i.e., the vertical flame below the target surface. After impingement, the flame extends outwards radially along the target surface, forming the horizontal wall jet flame.

Within the range of $S'$ from 4.56 to 9.12, both the open and impinging swirling IDF have little change in the flame appearance, such as the flame shape, size and color. Additionally, the flame structure identified is also similar. Therefore, only the case of $S'$ = 9.12 is enclosed in this paper. Basically, there are three types of flame structure for the impinging swirling IDF if the nozzle-to-surface distance is smaller than the flame height of the corresponding open swirling IDF, as shown in Fig. 4. Type I exits for $H/d \leqslant 2$ in which both Zones 1 and 2 impinge on the target surface, with a very small IRZ in the center. Recirculation as observed in the open swirling IDF is strongly suppressed by the target surface. The small

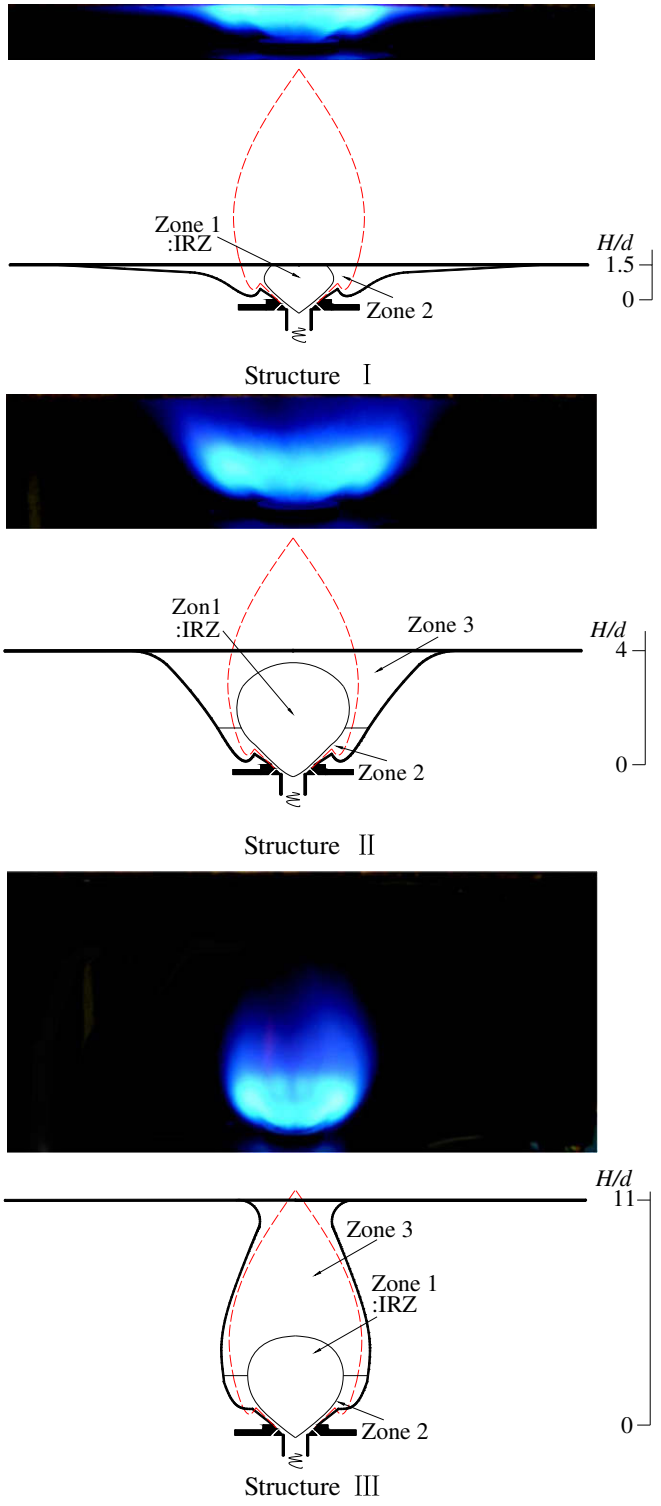


**Fig. 4.** Structures of impinging swirling IDFs at $Re$ = 8000, $\Phi$ = 1.4 and $S'$ = 9.12.

IRZ is formed by the inward flow diverged from the mainstream of the flame jet when it strikes on the target surface at a radial position near to the stagnation point. Type II arises for $2 < H/d \leqslant 9$ in which both Zones 1 and 3 impinge on the target surface, with a large IRZ in the center. Recirculation as observed in the open swirling IDF is slightly suppressed by the target surface. In both Type I and Type II flame structures, a portion of those fluid particles in the flame boundary (which recirculate in the case of the open swirling IDF) diverge outwards after colliding with the solid surface of the

copper plate, enforcing more chemical reactions to occur in the wall jet region, rather than in the IRZ of the open swirling IDF. Type III appears at a sufficiently large nozzle-to-surface distance, for instance $H/d = 11$, in which the flame below the target surface resembles the open swirling IDF in terms of flame structure. In Fig. 4, each sketch of the impinging swirling IDF is overlapped by the contour of the corresponding open swirling IDF, designated by dashed lines. From this direct comparison, the additional expansion of the vertical flame before impingement is clearly seen in Type I and Type II, and the additional expansion in the flame almost disappears in Type III.

### 3.2. Wall static pressure

The wall static pressure exerted by a flame jet on the target surface is closely correlated with the hydrodynamic characteristics of the flame jet [7]. In the present study, the radial distribution of the wall static pressure exerted by the impinging swirling IDF on the target surface, as measured by a micro-manometer, is shown in Fig. 5. The wall static pressure is proportional to the flow velocity normal to the impingement plate. Thus an increase in *Re* would lead to an increase in the wall static pressure.

Close to the stagnation point, the wall static pressure has negative values at $0.5 \leqslant H/d \leqslant 3$, indicating the presence of a reverse flow detaching away from the target surface. The stagnation point static pressure increases monotonically with increasing $H$ and attains positive values at $H/d = 4$ and above, indicating that the amount of flow being attached to the stagnation point is increasing as the target surface is elevated from the burner nozzle.

At each $H/d$ in the range of 0.5–2 where Type I flame structure exits and along the radial direction, the wall static pressure increases sharply to a peak value at a radial position corresponding to the vertical flame boundary where large quantities of fluid particles in Zone 2 impinge on the target surface and then decreases rapidly to nearly atmospheric pressure in the wall jet region. At each $H/d$ in the range of 3–9 where Type II flame structure arises, the wall static pressure attains peak values in the flame boundary again, and decays on both sides. It is also shown that as $H/d$ increases from 0.5 to 9, the peak value of the wall static pressure decreases monotonically with its position shifting farther away from the stagnation point. This is because mixing between the swirling jet and the ambient air causes velocity decay and expansion of the flame jet. The mixing also results in a thicker flame boundary at a higher $H$, as indicated by the widening span of the wall static pressure peak. At $H/d = 11$ where Type III flame structure appears, the wall static pressure displays no clear peak and just drops along the radial direction, indicating that post-combustion products converge and strike on the target surface uniformly.

### 3.3. Flame temperature

To measure the flame temperature, an uncoated type B thermocouple was mounted in the copper plate with the bead of the thermocouple located at a distance of 3 mm below the front side of the copper plate facing the flame. The recorded temperatures were corrected for radiation loss and are shown in Fig. 6.

At each $H/d$ in the range of 0.5–2, the peak of the flame temperature has a high value of about 1600 °C and the flame temperature peak is broad with its span much wider than that of the corresponding wall static pressure peak. This is because that the radial position of the peak flame temperature is slightly offset to the right side of the corresponding radial position of peak wall static pressure (to be slightly farther away from the stagnation point). Both fast mixing of the fuel with air and the intense chemical reactions take place in the vertical flame boundary such that the wall static pressure attains its peak value at the location where the flame boundary directly impinges on the target surface. After impingement and under the influence of the target surface, the majority of the fluid particles in the flame boundary diverge outwards radially. At short nozzle-to-surface distances, the outgoing fluid flow pushes some unburned fuel farther away from the stagnation point for further reactions with air. As a result, combustion is more intense slightly downstream of the flame boundary, generating the peak flame temperature at the right side of the pressure peak. Note that at $H/d = 0.5$, the flame temperature drops heavily to 982 °C at $R/d = 1.3$ ($R = 16$ mm), which is a position in the closest vicinity of the burner rim and where the wall static pressure is the highest. The decrease in flame temperature is due to the quenching effect induced by the burner rim.

As $H/d$ increases to 3 and further to 9, the peak flame temperature drops monotonically and its radial position shifts gradually from the right to the left side of the corresponding position of peak wall static pressure. The reason is that there is less unburned fuel being diverged outwards radially after impingement and thus complete combustion eventually occurs in the vertical flame boundary before impingement on the target surface. The decrease

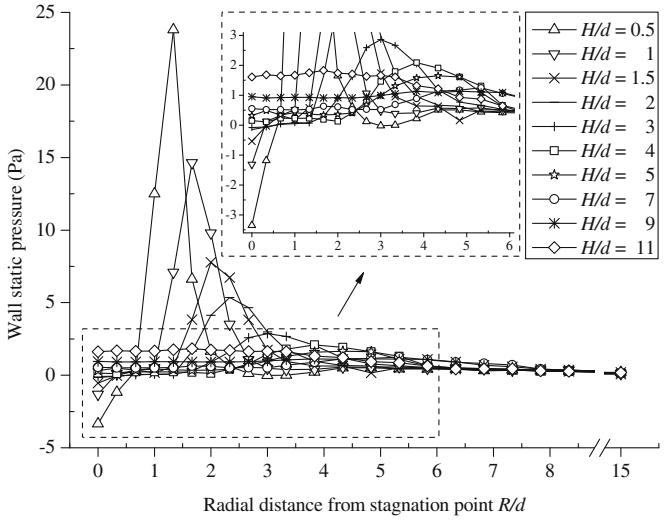


**Fig. 5.** Radial profiles of wall static pressure at different $H$, $Re = 8000$, $\Phi = 1.4$ and $S' = 9.12$.

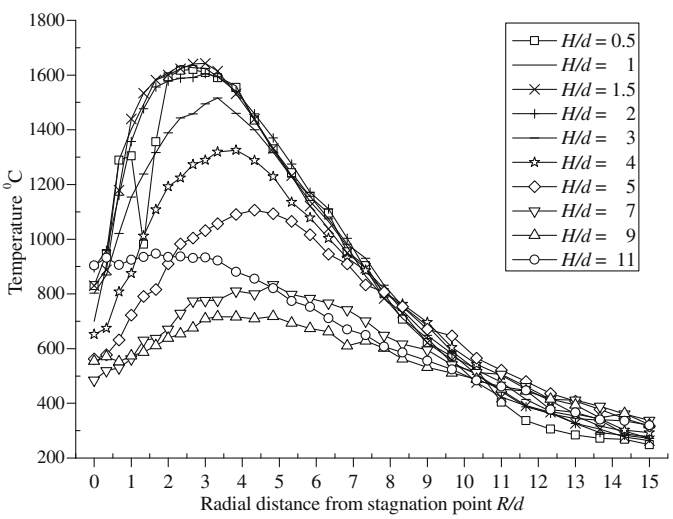


**Fig. 6.** Radial profiles of flame temperature at different $H$, $Re = 8000$, $\Phi = 1.4$ and $S' = 9.12$.

in the peak flame temperature is due to the mixing between the swirling jet and the ambient air leading to dilution and cooling down of the combustion products.

At $H/d = 11$ and in a broad region around the stagnation point, the flame temperature becomes higher than that at $H/d = 9$ and keeps rather uniform with no clear peak. The increase in flame temperature is the result of the alleviated dilution associated with the disappearance of the additional expansion in the flame, thus there is less dilution and cooling down of the combustion products.

### 3.4. Effect of H on the local heat flux

The effect of $H$ on the radial heat flux distribution investigated at $Re = 8000$, $\Phi = 1.4$ and $S' = 9.12$ is shown in Fig. 7. The profiles in Fig. 7 can be classified to three groups. The first group corresponds to $H/d = 0.5$–2, the second group pertains to $H/d = 3$–9 and the third group is for $H/d = 11$. As for the first group, Fig. 7 shows that, from the stagnation point to $R/d = 15$, it has double peaks at $H/d = 0.5$ and only single peak for other values of $H/d$. As $H/d$ increases, $h_{max}$, which is the peak value of the heat flux along each heat flux profile, firstly increases and then decreases with the maximum value obtained at $H/d = 1.5$. At small values of $H/d$ from 0.5 to 2, the bright-color reaction zone, i.e., Zone 2, is in contact with the target surface, and because of the intense combustion very high flame temperatures are formed in the flame boundary and slightly downstream, as shown in Fig. 6. Similar radial distributions of the flame temperature are observed except that at $H/d = 0.5$, the burner rim at $R/d = 1.3$ acts as a heat sink and reduces the flame temperature. Fig. 5 illustrates that the wall static pressure drops with the peak value decreasing from 24 Pa at $H/d = 0.5$ to 5 Pa at $H/d = 2$. Therefore, it is clear that the change in $h_{max}$ from $H/d = 0.5$ to 2 is due to the contribution of heat release from chemical reactions, which might be the maximum at $H/d = 1.5$.

With regard to the second group, Fig. 7 illustrates that the value of $h_{max}$ decreases monotonously from $H/d = 3$ to 9, while the position of $h_{max}$ shifts gradually farther away from the stagnation point. When $H/d$ exceeds 2, a sky-blue flame, i.e., Zone 3, emerges on the top of the bright-color reaction zone and gets in contact with the target surface. Furthermore, complete combustion tends to occur in the vertical flame boundary at $H/d > 2$. Thus the influence of heat release on the local heat flux could be assumed to be ignored and the decrease in $h_{max}$ from $H/d = 3$ to 9 is attributed to the decay of impinging velocity and flame temperature (incurred by mixing between the swirling jet and ambient air).

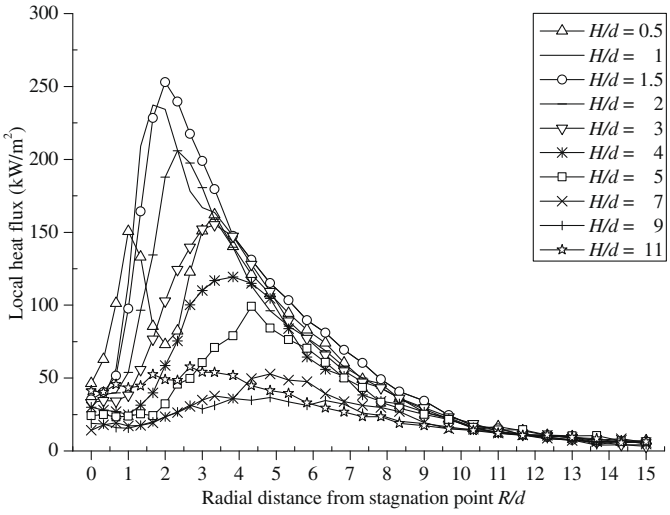


**Fig. 7.** Radial profiles of heat flux at different $H$, $Re = 8000$, $\Phi = 1.4$ and $S' = 9.12$.

As for the last group, i.e., at $H/d = 11$, Fig. 7 shows that in a broad region around the stagnation point, the local heat flux becomes substantially higher than that at $H/d = 9$, and remains uniform at $R/d < 3.3$. A transition in the flame structure from Type II to Type III occurs as $H/d$ increases from 9 to 11. At $H/d = 11$, the nozzle-to-surface distance is comparable to the flame height of the corresponding open swirling IDF, and the impinging IDF behaves similarly to the open IDF in that most of the fluid particles in Zone 3 converge towards the burner axis before impingement. Thus the additional expansion in the vertical flame disappears and upon impingement the fluid particles, which are mainly post-combustion products, are diverged outwards radially by the target surface. Because of the disappearance of the additional expansion, mixing between the swirling jet and the ambient cold air is reduced, and both flame temperature and impinging velocity are recovered to a certain extent, bringing increases to the local heat flux.

In the far wall jet region, as shown in Fig. 7, there is little difference among the radial heat flux profiles, illustrating that combustion has reached completion and it is the combustion products which form a hot gas layer that heats up the target surface.

In conclusion, the swirling effect influences heat transfer in three ways. Firstly, the heat transfer at the stagnation point is severely deteriorated by swirl. Secondly, both high impinging velocity and high flame temperature dwell in the flame boundary, and the local heat flux is the highest at a certain radial position, following the position of either the peak impinging velocity or the peak flame temperature. Thirdly, as $H$ increases, the swirling jet brings the position of $h_{max}$ gradually farther away from the stagnation point.

Based on Eqs. (2) and (3), the area-integrated heat flux or the overall heat transfer rate and the heat transfer efficiency of different $H$ at $Re = 8000$, $\Phi = 1.4$ and $S' = 9.12$ are calculated and shown in Fig. 8(a). It is seen that the overall heat transfer rate $\dot{q}$ increases from 3.64 kW at $H/d = 0.5$ to 4.27 kW at $H/d = 1.5$, decreases to 1.72 kW at $H/d = 9$ and increases slightly to 1.89 kW at $H/d = 11$. Since both $Re$ and $\Phi$ are fixed, the heat transfer efficiency and the overall heat transfer rate have the same trend of variation with $H$. Therefore, both the maximum $\dot{q}$ and the maximum $\eta$ occurring at $H/d = 1.5$ mean that this is the optimum nozzle-to-surface distance for the operational condition of $Re = 8000$, $\Phi = 1.4$ and $S' = 9.12$ to exploit the swirling flow for the highest overall heat transfer rate and efficiency. To confirm that there exists an optimum nozzle-to-surface distance $H_{optimum}$ for the highest overall heat transfer rate and efficiency at other operational conditions, experiments were repeated at $Re = 8000$, $\Phi = 1.2$ and $S' = 9.12$, and $Re = 8000$, $\Phi = 1.6$ and $S' = 9.12$, respectively. The results showed that $H/d_{optimum} = 1$ for the former case and $H/d_{optimum} = 2$ for the latter case.

### 3.5. Effect of Φ on the local heat flux

The effect of $\Phi$ on the radial heat flux distribution investigated at $Re = 8000$, $H/d = 1.5$, and $S' = 9.12$ is shown in Fig. 9. The local heat flux along each profile is very low at the stagnation point, increases steeply to a peak value in the radial direction and then drops gradually in the wall jet region. As mentioned earlier, this pattern of radial heat flux distribution is due to the swirling effect. The six profiles overlap each other in the region close to the stagnation point, depart towards reaching their different peaks, and differ very much despite following the same trend of decline in the wall jet region.

As $\Phi$ changes in the range of $1.0 \leqslant \Phi \leqslant 2.0$ and close to the stagnation point, the profiles overlap each other, showing that the stagnation point heat transfer remains severely suppressed by the swirling effect and thus the influence of $\Phi$ on the radial distribution of the local heat flux is negligibly small is this region. The profiles

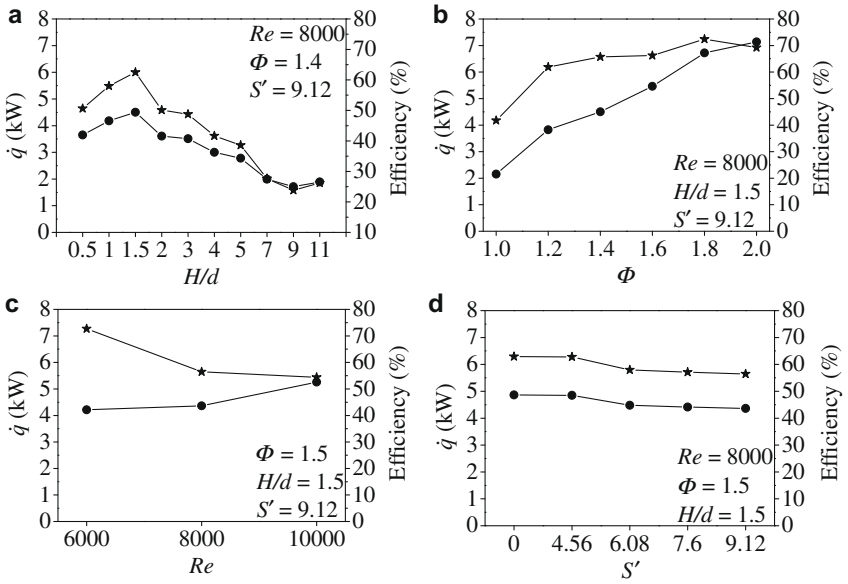


**Fig. 8.** Variation of overall heat transfer rate and heat transfer efficiency with operational parameters: (a) $H/d$; (b) $\Phi$; (c) $Re$; (d) $S'$; '●' for overall heat transfer rate and '★'for heat transfer efficiency.

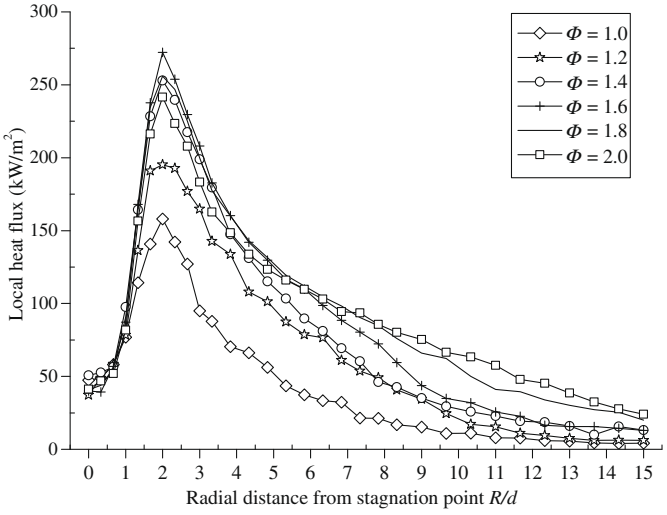


**Fig. 9.** Radial profiles of heat flux at different $\Phi$, $Re = 8000$, $H/d = 1.5$ and $S' = 9.12$.

exhibit a large variation in the value of $h_{max}$ which first increases and then decreases since the increasing value of $\Phi$ from 1.0 to 2.0 leads the actual flame to fuel-lean, stoichiometric and fuel-rich conditions, resulting in the maximum $h_{max}$ attained at $\Phi = 1.6$. However, $h_{max}$ occurs at nearly the same location of $R/d = 2$, which indicates that there is little change in the hydrodynamic characteristics of the impinging flame jet. After reaching their peaks, these profiles decline steadily and the rate at which a profile declines is lower at higher $\Phi$ in the wall jet region, manifesting much difference in the local heat flux in this region. The reason is that when $\Phi$ increases, there is more unburned fuel pushed outwards radially to react with air in the wall jet region and therefore the flame temperature in this region tends to increase and the local heat flux becomes higher.

The overall heat transfer rate and the heat transfer efficiency of different $\Phi$, at $Re = 8000$, $H/d = 1.5$ and $S' = 9.12$ are shown in Fig. 8(b). An increase in $\Phi$ at a fixed $Re$ means that the fuel flow rate is increasing while the air flow rate is fixed. Therefore, the value of $\dot{q}$ increases monotonically from 2.15 kW at $\Phi = 1.0$ to 7.14 kW at $\Phi = 2.0$, due to the increasing energy input. The maximum heat transfer efficiency occurs around $\Phi = 1.8$ and drops on both ends. This result is similar to the findings in Ref. [8], which studied in details the efficiency of the heat transfer process of a non-swirling IDF, and stated that at fixed $Re$ and $H$, the heat transfer efficiency increases to a maximum value and then decreases as $\Phi$ increases.

### 3.6. Effect of Re on the local heat flux

The effect of $Re$ on the radial heat flux distribution investigated at $\Phi = 1.5$, $H/d = 1.5$ and $S' = 9.12$ is shown in Fig. 10. The local heat flux in both the stagnation region and the wall jet region increases as $Re$ increases from 6000 to 10000. The radial position of $h_{max}$ is invariant at $R/d = 2$. Thus, $H$ is the key parameter in affecting the radial position of $h_{max}$, compared with $Re$ and $\Phi$. The increase in the local heat flux is because that a higher fuel flow rate is associ-

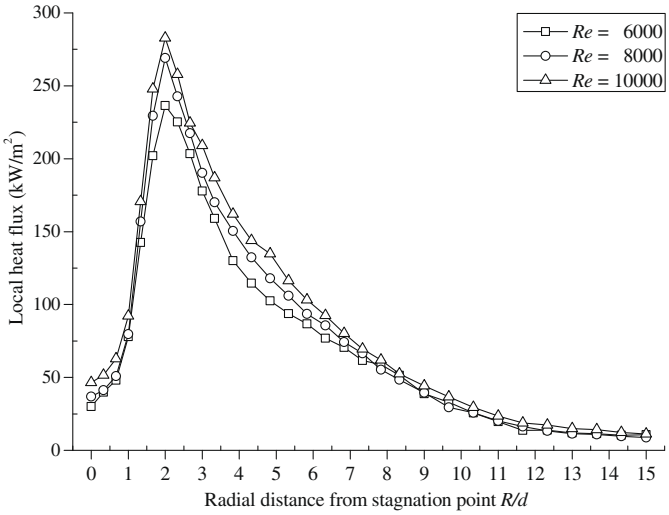


**Fig. 10.** Radial profiles of heat flux at different $Re$, $\Phi = 1.5$, $H/d = 1.5$ and $S' = 9.12$.

ated with a higher $Re$ while $\Phi$ is kept unchanged, which leads to more heat released. Further, a higher $Re$ generally induces higher impinging velocity, better mixing of the fuel/air, higher level of turbulence and thus higher flame temperature, all of which could enhance the heat transfer rates.

The overall heat transfer rate and the heat transfer efficiency of different $Re$, at $\Phi = 1.5$, $H/d = 1.5$ and $S' = 9.12$ are shown in Fig. 8(c). An increase in $Re$ at a fixed $\Phi$ means that both the fuel and air flow rates are increasing, so that there is an increase in the energy input to the flame impingement system and therefore the overall heat transfer rate $\dot{q}$ increases monotonously from 4.21 kW at $Re = 6000$ to 5.26 kW at $Re = 10{,}000$. On the contrary, the heat transfer efficiency decreases as $Re$ increases. This result is also similar to that in Ref. [8]. Ref. [8] attributed the decreasing efficiency with $Re$ to that more energy is transferred beyond the integration area, which might not be true in this study because of the different range of $Re$ between the two studies. The possible reason in the current study is more related to the increase in the amount of entrained ambient air at a higher $Re$. The entrained ambient cold air absorbs a significant amount of energy and takes away a larger portion of heat such that the portion to the target surface is reduced.

### 3.7. Effect of $S'$ on the local heat flux

The degree of swirl was altered by adjusting the relative magnitude of tangential and axial flow rates of air for the swirling IDF burner. For guarantee of the formation of the IRZ in the swirling IDF, the adjustment of swirl number was restricted to the high-swirl range of $4.56 \leqslant S' \leqslant 9.12$. The effect of $S'$ on the radial heat flux distribution investigated at $Re = 8000$, $\Phi = 1.5$ and $H/d = 1.5$ is shown in Fig. 11.

Generally, a higher swirl number tends to move the radial position of $h_{max}$ outwards radially because of a higher jet spreading rate. In the study of Owsenek et al. [18], the radial position of $h_{max}$ is situated markedly further away from the stagnation point when the actual swirl number $S$ increases from 0.21 to 0.77. However in this study, the displacement of the radial position of $h_{max}$ is not observed at $H/d = 1.5$ and in the range of $4.56 \leqslant S' \leqslant 9.12$, probably because the divergent outlet of the swirling IDF burner confines the evolution of the swirling jet at short nozzle-to-surface distances. In other words, the centrifugal force induced by such high-swirl intensity is so strong that the swirling jet flow follows the curvature of the divergent outlet, which is 45° in this study.

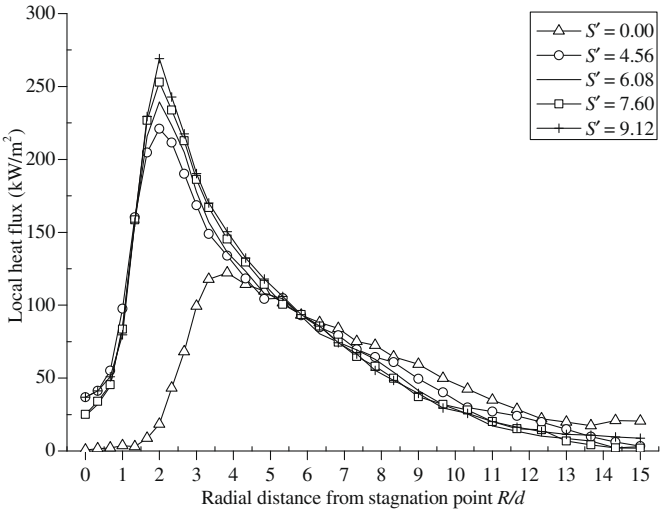


**Fig. 11.** Radial profiles of heat flux at different $S'$, $Re = 1.5$, $\Phi = 8000$, and $H/d = 1.5$.

As shown in Fig. 11, the radial position of $h_{max}$ is maintained at $R/d = 2$, and the value of $h_{max}$ increases monotonically as $S'$ increases from 4.56 to 9.12, which might be due to the higher flame temperature associated with better mixing of the fuel with air and higher level of turbulence induced by the higher $S'$. Except the difference in the value of $h_{max}$, the other parts of the profiles are close to each other, with the local heat flux in the wall jet region being slightly lower at a higher $S'$. Moreover, as $S'$ increases, there is a slight decrease in the overall heat transfer rate, as shown in Fig. 8(d), decreasing monotonically from 4.85 to 4.36 kW as $S'$ increases from 4.56 to 9.12. Thus there is no enhancement in heat transfer caused by the elevated $h_{max}$ and actually the overall heat transfer rate decreases with $S'$, which shows a negative effect of swirl on heat transfer. Fig. 8(d) also shows that the heat transfer efficiency decreases with increasing $S'$, which is evidence that the swirl has an unfavorable effect on heat transfer.

Non-swirling IDFs have been extensively investigated in Refs. [6–8,12]. In the present study, a non-swirling IDF with a swirl number of $S' = 0$ was generated by setting the tangential air flow rate to zero. The impinging non-swirling IDF exhibits similar behaviour to that of IDFs studied in the literature. At small nozzle-to-surface distances, there exists a cool core in the centre of the flame adjacent to the burner exit. The cool core mainly consists of air supplied from the central air port and leads to very low heat flux in the stagnation region. The cool core gradually disappears as complete combustion is reached at higher nozzle-to-surface distances, displaying a bell-shaped radial heat flux distribution. At even higher $H$, the local heat flux drops as combustion products heat up the target surface. The radial heat flux profile at $Re = 8000$, $\Phi = 1.5$, $H/d = 1.5$ and $S' = 0$ is also shown in Fig. 11. The nearly zero heat flux in the vicinity of the stagnation point is dictated by the cool core. The radial position of $h_{max}$ is at $R/d = 3.8$ instead of $R/d = 2$ for the swirling IDFs and the value of $h_{max}$ is 122 kW/m$^2$ which is much lower than those for the swirling IDFs. This illustrates that the induced-swirl promotes rapid mixing of the fuel/air and boosts intense combustion so that the cool core present in the case of the non-swirling IDF disappears when swirl is introduced. Thus, the swirling IDF achieves complete combustion at a lower $H$, when compared with the non-swirling IDF. At $R/d > 5.8$, the local heat flux of the non-swirling IDF becomes higher than that of the swirling IDFs. This shows that because of less intense mixing between the fuel and air in the non-swirling IDF, more unburned fuel is forced to the wall jet region for further reactions with air. This particularly higher heat flux in the wall jet region makes the non-swirling IDF possess an overall heat transfer rate higher than those of the swirling IDFs. As shown in Fig. 8(d), the overall heat transfer rate for the non-swirling IDF at $S' = 0$ has an overall heat transfer rate of 4.86 kW which is higher than those of the swirling IDFs. The heat transfer efficiency of the non-swirling IDF is also higher than those of the swirling IDFs, as shown in Fig. 8(d).

Ng et al. [8] suggested that for achieving the highest overall heat transfer rate, the value of $H$ should correspond to the range of complete combustion region. In this study, the non-swirling IDF operating at $Re = 8000$ and $\Phi = 1.4$ achieves complete combustion at $H/d = 6$ and attains the highest overall heat transfer rate of 5.73 kW, with a bell-shaped radial heat flux distribution and $h_{max} = 267$ kW/m$^2$ occurring at the stagnation point. From the finding mentioned earlier, for the swirling IDF at $Re = 8000$, $\Phi = 1.4$ and $S' = 9.12$, $H/d_{optimum} = 1.5$. Thus a comparison of the highest overall heat transfer rates of impinging swirling and non-swirling IDFs at their individual optimum nozzle-to-surface distances is conducted and shows that the swirl has an adverse effect on heat transfer and reduces the overall heat transfer rate. The reduction from 5.73 kW of the non-swirling IDF at $H/d_{optimum} = 6$ to 4.27 kW of the swirling IDF at $H/d_{optimum} = 1.5$ is as high as 25%.

## 4. Conclusions

An experimental study was carried out to investigate the heat transfer characteristics of a turbulent and swirling inverse diffusion flame (IDF) impinging vertically normal to a flat surface. The swirling effect and the effects of different operational parameters including Reynolds number, overall equivalence ratio, nozzle-to-surface distance and swirl number on the local heat flux distributions were examined. The comparison of heat transfer of impinging IDFs with and without swirl was also conducted.

The experimental results revealed that the swirling effect affects the distribution of local heat flux in three ways. (1) The heat transfer at the stagnation point deteriorates to some extent and rises in the radial direction. (2) The peak of local heat flux occurs at a radial distance from the stagnation point where the vertical flame boundary strikes on the target surface or slightly downstream. (3) The radial position of peak local heat flux shifts farther away from the stagnation point as $H$ increases.

Based on the open swirling IDF whose flow field was visualized by a visualization technique developed by the author, the structure of the impinging swirling IDF was grouped into three types. Flame temperature is the main factor that influences heat transfer in all cases. At each combination of $Re$, $\Phi$ and $S'$, there exists an optimum $H$ which yields the highest overall heat transfer rate, and $H_{\text{optimum}}$ becomes higher with increasing $\Phi$ while $Re$ and $S'$ are kept unchanged. The investigation of effects of operational parameters on heat transfer showed that the overall heat transfer rate increases when either $Re$ or $\Phi$ is increased with other parameters unchanged, and that the overall heat transfer rate decreases when $S'$ increases with $Re$, $\Phi$ and $H$ unchanged. The heat transfer efficiency is found to be more useful in indicating the effectiveness of energy transferred from the flame to the target surface. At fixed $Re$, $\Phi$ and $S'$, the highest heat transfer efficiency occurs at $H_{\text{optimum}}$ pertaining to the highest overall heat transfer rate. At fixed $Re$, $H$ and $S'$, there exists an optimum $\Phi$ for the highest efficiency. At fixed $\Phi$, $H$ and $S'$, a higher $Re$ yields a lower efficiency. At fixed $Re$, $\Phi$ and $H$, a higher $S'$ produces a lower efficiency.

The comparison of IDFs showed that the impinging swirling IDF achieves complete and intense combustion at smaller nozzle-to-surface distances, compared with the impinging non-swirling IDF, due to better mixing between the fuel and air induced by the swirl. It is obvious that the introduction of swirl shifts the region of complete combustion to lower nozzle-to-surface distances. Therefore, the value of $H_{\text{optimum}}$ pertaining to the highest overall heat transfer rate is smaller in the case of the impinging swirling IDF. However, the highest overall heat transfer rate is much lower, illustrating an unfavorable effect of swirl on heat transfer.

## Acknowledgement

The authors wish to thank the Hong Kong Polytechnic University for financial support of the present study.

## References

[1] K. Jambunathan, E. Lai, M.A. Moss, B.L. Button, A review of heat transfer data for single circular jet impingement, Int. J. Heat Fluid Flow 13 (1992) 106–115.
[2] C.E. Baukal, B. Gebhart, A review of flame impingement heat transfer studies—Part 1. Experimental conditions, Combust. Sci. Technol. 104 (1995) 339–357.
[3] C.E. Baukal, B. Gebhart, A review of flame impingement heat transfer studies—Part 2. Measurements, Combust. Sci. Technol. 104 (1995) 359–385.
[4] S. Chander, A. Ray, Flame impingement heat transfer: a review, Energy Convers. Manage. 46 (2005) 2803–2837.
[5] G.K. Hargrave, M. Fairweather, J.K. Kilham, Forced convective heat transfer from premixed flames—Part 1. Flame structure, Int. J. Heat Fluid Flow 8 (1987) 55–63.
[6] L.L. Dong, C.S. Cheung, C.W. Leung, Heat transfer characteristics of an impinging inverse diffusion flame jet—Part 1. Free flame structure, Int. J. Heat Mass Transfer 50 (2007) 5108–5123.
[7] L.L. Dong, C.S. Cheung, C.W. Leung, Heat transfer characteristics of an impinging inverse diffusion flame jet—Part II. Impinging flame structure and impingement heat transfer, Int. J. Heat Mass Transfer 50 (2007) 5124–5138.
[8] T.K. Ng, C.W. Leung, C.S. Leung, Experimental investigation on the heat transfer of an impinging inverse diffusion flame, Int. J. Heat Mass Transfer 50 (2007) 3366–3375.
[9] M.E. Horsley, M.R.I. Purvis, A.S. Tariq, Convective heat transfer from laminar and turbulent premixed flames, Heat Transfer 3 (1982) 409–415.
[10] G.K. Hargrave, M. Fairweather, J.K. Kilham, Forced convective heat transfer from premixed flames—Part 2. Impingement heat transfer, Int. J. Heat Fluid Flow 8 (1987) 132–138.
[11] L.C. Kwok, C.W. Leung, C.S. Cheung, Heat transfer characteristics of slot and round premixed impinging flame jets, Exp. Heat Transfer 16 (2003) 111–137.
[12] L.K. Sze, C.S. Cheung, C.W. Leung, Temperature distribution and heat transfer characteristics of an inverse diffusion flame with circumferentially arranged fuel ports, Int. J. Heat Mass Transfer 47 (2004) 3119–3129.
[13] J.W. Mohr, J. Seyed-Yagoobi, R.H. Page, Combustion measurements from an impinging radial jet reattachment flame, Combust. Flame 106 (1996) 69–80.
[14] L.L. Dong, C.W. Leung, C.S. Cheung, Combustion optimization of a slot flame jet impinging system, J. Inst. Energy 76 (2003) 80–88.
[15] J. Ward, M. Mahmood, Heat transfer from a turbulent, swirling, impinging jet, Proceedings of the Seventh International Heat Transfer Conference, 1982, pp. 401–407.
[16] J. Ward, M. Mahmood, The effect of swirl on mass/heat transfer from arrays of turbulent, impinging jets, Proceedings of ASME-WAM, 1993, pp. 57–64.
[17] L. Huang, M.S. El-Genk, Heat transfer and flow visualization experiments of swirling, multi-channel, and conventional impinging jets, Int. J. Heat Mass Transfer 41 (1997) 583–600.
[18] B.L. Owsenek, T. Cziesla, N.K. Mitra, G. Biswas, Numerical investigation of heat transfer in impinging axial and radial jets with superimposed swirl, Int. J. Heat Mass Transfer 40 (1997) 141–147.
[19] D.H. Lee, S.Y. Won, Y.T. Kim, Y.S. Chung, Turbulent heat transfer from a flat surface to a swirling round impinging jet, Int. J. Heat Mass Transfer 45 (2002) 223–227.
[20] Z.X. Yuan, Y.Y. Chen, J.G. Jiang, C.F. Ma, Swirling effect of jet impingement on heat transfer from a flat surface to $CO_2$ stream, Exp. Thermal Fluid Sci. 31 (2006) 55–60.
[21] X.Q. Huang, C.W. Leung, C.K. Chan, S.D. Probert, Thermal characteristics of a premixed impinging circular laminar-flame jet with induced swirl, Appl. Energy 83 (2006) 401–411.
[22] Z. Zhao, D.W. Yuen, C.W. Leung, T.T. Wong, Thermal performance of a premixed impinging circular flame jet array with induced-swirl, Appl. Therm. Eng. 29 (2008) 159–166.
[23] N. Syred, J.M. Beer, Combustion in swirling flows: a review, Combust. Flame 23 (1974) 143–201.
[24] T.C. Claypole, N. Syred, The effect of swirl burner aerodynamics on $NO_x$ formation, Proceedings of the 18th International Symposium on Combustion, The Combustion Institute, 1981, pp. 81–89.
[25] S.J. Kline, F.A. McClintock, Describing uncertainties in single-sample experiments of temperature in flames, Mech. Eng. 74 (1993) 3–8.
[26] J. Ji, J.P. Gore, Flow structure in lean premixed swirling combustion, Proceedings of the Combustion Institute, 2002, pp.861–867.